Interferometric imaging condition for wave-equation migration

Paul Sava, Colorado School of Mines, and Oleg Poliannikov, Colorado University*

SUMMARY

The fidelity of depth seismic imaging depends on the accuracy of the velocity models used for wavefield reconstruction. Models can be decomposed in two components corresponding to large scale and small scale variations. In practice, the large scale velocity model component can be estimated with high accuracy using repeated migration/tomography cycles, but the small scale component cannot. Therefore, wavefield reconstruction does not completely describe the recorded data and migrated images are perturbed by artifacts.

There are two possible ways to address this problem: improve wavefield reconstruction by estimating more accurate velocity models and image using conventional techniques (e.g. wavefield cross-correlation), or reconstruct wavefields with conventional methods using the known smooth velocity model, and improve the imaging condition to alleviate the artifacts caused by the imprecise reconstruction, as suggested in this paper.

In this paper, the unknown component of the velocity model is described as a random function with local spatial correlations. Imaging data perturbed by such random variations is characterized by statistical instability, i.e. various wavefield components image at wrong locations that depend on the actual realization of the random model. Statistical stability can be achieved by local wavefield averaging either in spatial windows defined in the vicinity of the data acquisition locations, or in local windows defined in the vicinity of image points. We use the latter approach and show that the technique is effective in attenuating imaging artifacts without being hampered by some of the limitations of data-space alternatives.

INTRODUCTION

Seismic imaging in complex media requires accurate knowledge of the medium velocity. Assuming single scattering, imaging requires propagation of the recorded wavefields from the acquisition surface, followed by the application of an imaging condition highlighting locations where scattering occurs, i.e. where reflectors are present.

The main requirement for good-quality imaging is accurate knowledge of the velocity model. Errors in the model used for imaging lead to inaccurate reconstruction of the seismic wavefields and to distortions of the migrated images. In a realistic seismic experiment the velocity model is not known exactly. Migration velocity analysis produces large scale approximations of the model, but fine scale variations remain elusive. Therefore, even if the broad kinematics of the seismic wavefields are reconstructed correctly, the extrapolated wavefields also contain distortions that lead to image artifacts obstructing the image of the geologic structure under consideration. While it is certainly true that even the recovery of a long-wave background may prove to be a challenge in some circumstances, we do not attempt to address that issue in this paper. Instead, we concentrate solely on the problem of dealing with the effect of small scale random variations.

There are two ways in which we can approach this problem: The first option is to improve the velocity analysis methods to estimate the small-scale variations in the model. Such techniques take advantage of all information contained in seismic wavefields and are not limited to kinematic information of selected events picked from the data. Examples of techniques in this category are waveform inversion (Tarantola, 1987; Pratt and Worthington, 1990; Pratt, 1990), wave-equation tomography (Woodward, 1992) or wave-equation migration velocity analysis (Sava and Biondi, 2004a,b; Shen et al., 2005). A more accurate velocity model allows for more accurate wavefield reconstruction. Then, wavefields can be used for imaging using conventional procedures, e.g. cross-correlation.The second option is to concentrate on the imaging condition, rather than concentrate on wavefield reconstruction. Assuming that the large-scale component of the velocity models is known (e.g. by iterative migration/tomography cycles), we can design imaging conditions that are not sensitive to small inaccuracies of the reconstructed wavefields. Imaging artifacts can be reduced at the imaging condition step, despite the fact that the wavefields incorporate small kinematic errors due to velocity fluctuations. The two options are complementary to each other, and both can contribute to imaging accuracy.

Conventional imaging consists of cross-correlations of extrapolated source and receiver wavefields at image locations. Since wavefield extrapolation is performed using an approximation of the true model, the wavefields contain random time delays, or equivalently random phases, which lead to imaging instability expressed as artifacts.

Statistical stability can be achieved if random phase shifts between signals recorded at nearby locations are removed by cross-correlation, prior to back propagation into the medium. This observation lies at the heart of coherent interferometric imaging (Borcea et al., 2005, 2006a,b,c) or imaging and velocity analysis in presence of uncertain models (Dussaud, 2005). We investigate an alternative way of using time reversal to increase imaging statistical stability. Instead of coherent interferometry applied to data on the acquisition surface, we first extrapolate wavefields to all locations in the imaging volume and then apply local spatial cross-correlations in the vicinity of every image point. Correlations in the image-space damps small random fluctuations in the extrapolated wavefields. The cross-correlations do not relocate energy in space, but simply produce local averages of the extrapolated wavefields.

The procedure closely resemble conventional imaging procedures where wavefields are extrapolated in the image volume and then cross-correlated in time at every image location. Our method uses averaging in three-dimensional local windows around image locations. From implementation and computational cost points of view, our technique does not differ much from conventional imaging, although the imaging properties are improved. We use the name *interferometric imaging condition* for our technique to contrast it with conventional imaging condition which represents a special case for infinitely small local windows.

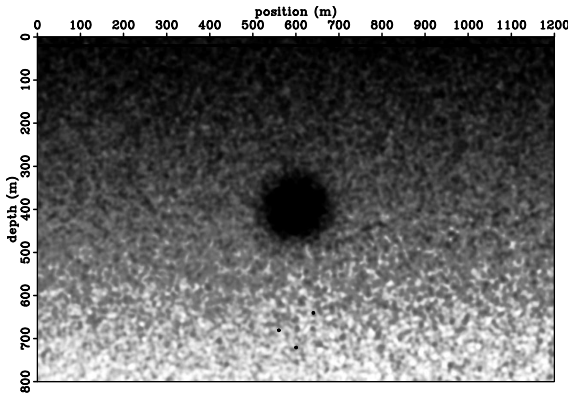

Figure 1: Velocity model with random variations. Imaging targets are 3 point sources located around $x = 600$ m, $z = 700$ m.

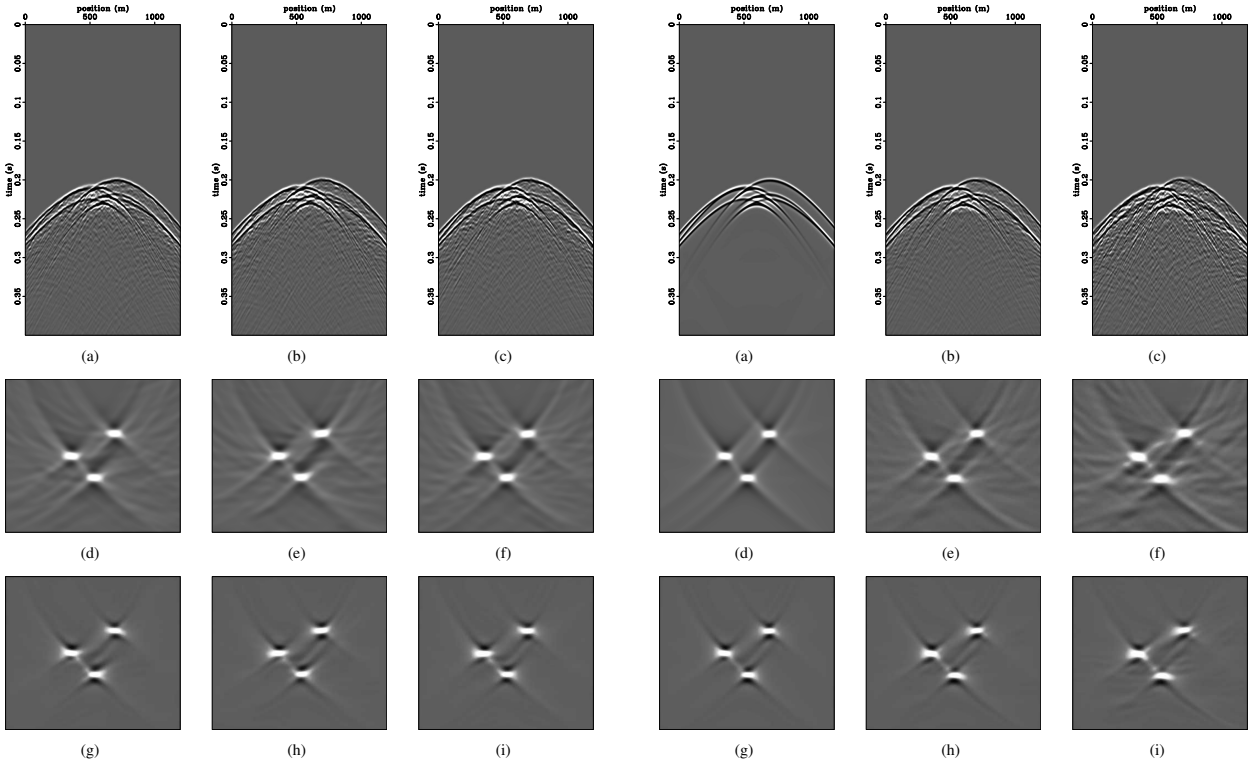

Figure 2: Illustration of statistical stability for the interferometric imaging condition in presence of random model variations. Data modeled with velocity with random variations with magnitude $\sigma = 20\%$, for different realizations of the noise model n. Images obtained by conventional imaging (d)-(f) and images obtained by interferometric imaging (g)-(i).

Figure 3: Illustration of interferometric imaging condition robustness in presence of random model variations. Data modeled with velocity with random variations with magnitude $\sigma = 0\%$ (a), $\sigma = 15\%$ (b), and $\sigma = 30\%$ (c). Images obtained by conventional imaging (d)-(f) and images obtained by interferometric imaging (g)-(i).

THEORY

Conventional seismic imaging is a two-step procedure: The first step consists of extrapolation of source and receiver wavefields from the recording surface to image locations. The source wavefield corresponds to simulated waves propagating forward in time from the source location $\mathbf{x}_s$, and the receiver wavefield corresponds to waves propagating backward in time from recording locations $\mathbf{x}_m$. The second step consists of an imaging condition evaluating whether the two extrapolated wavefields match kinematically, which indicates whether a reflector is present in the medium.

Wavefield extrapolation and imaging can be implemented in different space and time domains, for example downward continuation with the one-way wave-equation implemented in frequency-wavenumber, frequency-space or mixed domains, or wavefield extrapolation with the two-way wave-equation in time-space, etc. However, the actual extrapolation method is irrelevant for the discussion in this paper.

Conventional imaging condition (CIC)
The conventional way of implementing the imaging condition for wave-equation migration involves cross-correlation of the source and receiver wavefields, often referred to as the $U\overline{D}$ imaging condition (Claerbout, 1985), where D and U stand for downward and upward propagating wavefields. The image R is evaluated using the relation

$$R(\mathbf{y}_m) = \int\limits_{\omega_m} d\omega_m \, \overline{U_S(\mathbf{x}_s, \mathbf{y}_m, \omega_m)} \int\limits_{\mathbf{x}_m} d\mathbf{x}_m \, U_R(\mathbf{x}_m, \mathbf{y}_m, \omega_m) \ , \qquad (1)$$

where $U_S(\mathbf{x}_s, \mathbf{y}_m, \omega_m)$ represents the source wavefield at coordinates $\mathbf{y}_m$ simulated from a source at coordinates $\mathbf{x}_s$ and $U_R(\mathbf{x}_m, \mathbf{y}_m, \omega_m)$ represents the receiver wavefield reconstructed at coordinates $\mathbf{y}_m$ from the recorded data at coordinates $\mathbf{x}_m$. The summation over frequency ω_m implements the zero cross-correlation lag imaging condition. Here and for the rest of the paper, summation over multiple seismic experiments (sources) is assumed.

The assumption made in this model is that the Green's functions used for reconstruction are accurate representations of the Green's functions describing wave propagation in the real medium. However, for the case of media with random velocity fluctuations, v_0 is a smooth velocity approximating v. Thus, although the general kinematics of wave propagation are accurately described by v_0, the velocity fluctuations induce perturbations of the wavefield leading to imaging artifacts.

Coherent interferometric imaging
One way of addressing the problem of imaging in models with random fluctuations involves statistical stabilization using phase compensation in windows localized in time and space (Papanicolaou et al., 2004; Fouque et al., 2005). The idea is that small wavefield fluctuations caused by random perturbations of the velocity model are incoherent spatially and temporally and cancel-out by local cross-correlation and averaging.

The idea of statistical stability for imaging in random media is exploited by the technique called *coherent interferometric imaging* (Borcea et al., 2006b). The main idea of this method is to reduce the delay spread caused by the random fluctuations of the medium using averages of local cross-correlations between nearby traces on the acquisi-

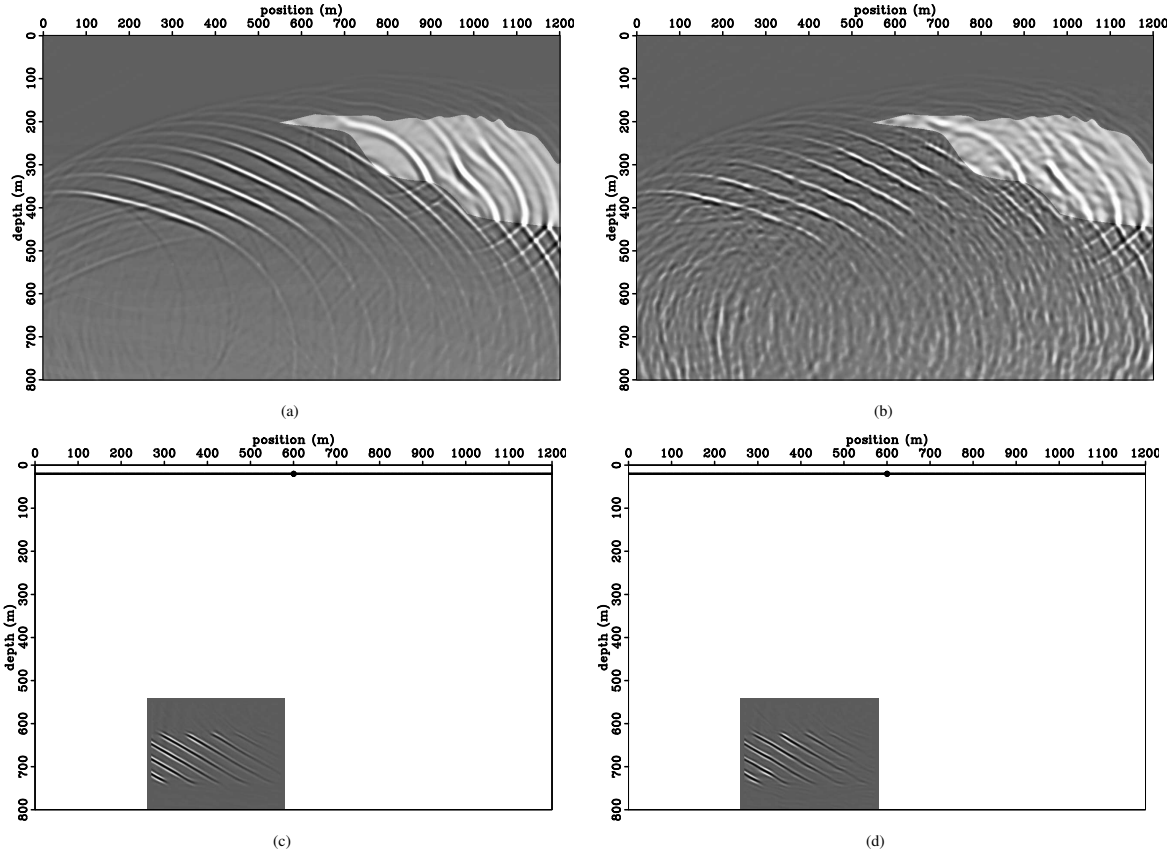

Figure 4: Overlay of reflected wavefield on background velocity model (a) and on velocity model with random variations (b). Image produced by reverse-time migration using the background velocity model for data simulated in the background model (c) and for data simulated in the model with random variations (d). Enlarged images are shown in figures 5(a)-5(d).

tion surface. The coherent interferometric imaging functional is

$$R(\mathbf{y}_m) = \int\limits_{\omega_m} d\omega_m \int\limits_{|\omega_h|\le\Omega/2} d\omega_h \int\limits_{\mathbf{x}_m} d\mathbf{x}_m \int\limits_{|\mathbf{x}_h|\le X/2} d\mathbf{x}_h \frac{\overline{U_S(\mathbf{x}_s,\mathbf{y}_m,\omega_m-\omega_h)}\,U_R(\mathbf{x}_m-\mathbf{x}_h,\mathbf{y}_m,\omega_m-\omega_h)}{\overline{U_S(\mathbf{x}_s,\mathbf{y}_m,\omega_m+\omega_h)}\,U_R(\mathbf{x}_m+\mathbf{x}_h,\mathbf{y}_m,\omega_m+\omega_h)} \qquad (2)$$

where $\mathbf{x}_h$ represents a 2D summation variable on the acquisition surface in a window of size X called decoherence length, and ω_h represents a summation variable along the frequency axis in a window of size Ω called decoherence frequency.

Interferometric imaging condition (IIC)

An alternative approach to coherent imaging is to reconstruct wavefields at all locations in the imaging volume from all locations on the acquisition surface and suppress the random fluctuations in the wavefield by local cross-correlations in windows around image points.

For coherent imaging after extrapolation, we can define another 3D decoherence length around an image point Y, which is analogous to the 2D decoherence length defined on the acquisition surface X. The imaging functional for this case is

$$R(\mathbf{y}_m) = \int\limits_{\omega_m} d\omega_m \int\limits_{|\omega_h|\le\Omega/2} d\omega_h \int\limits_{|\mathbf{y}_h|\le Y/2} d\mathbf{y}_h \frac{}{\overline{U_S(\mathbf{x}_s,\mathbf{y}_m-\mathbf{y}_h,\omega_m-\omega_h)}\int\limits_{\mathbf{x}_m} d\mathbf{x}_m\, U_R(\mathbf{x}_m,\mathbf{y}_m-\mathbf{y}_h,\omega_m-\omega_h)}$$

$$\overline{U_S(\mathbf{x}_s,\mathbf{y}_m+\mathbf{y}_h,\omega_m+\omega_h)}\int\limits_{\mathbf{x}_m} d\mathbf{x}_m\, U_R(\mathbf{x}_m,\mathbf{y}_m+\mathbf{y}_h,\omega_m+\omega_h) \qquad (3)$$

where $\mathbf{y}_h$ represents a 3D summation variable around the image point. We can describe the imaging method summarized by equation (3) by the name *interferometric imaging condition*, since it acts similarly to the conventional imaging condition, but with robustness with respect to random fluctuations due to local interferometric averaging in windows around image locations.

Comparison of imaging functionals

At first glance, the imaging functionals (2) and (3) look similar in shape and imaging properties. However, from a practical point of view, the two imaging functionals are fundamentally different. Imaging functional (2) achieves statistical stability by cross-correlating and averaging wavefields parametrized function of the location of receivers on the acquisition surface. In this functional, the wavefields subject to cross-correlation are $\overline{U_S(\mathbf{x}_s,\mathbf{y}_m,\omega_m\pm\omega_h)}U_R(\mathbf{x}_m\pm\mathbf{x}_h,\mathbf{y}_m,\omega_m\pm\omega_h)$. This operation requires that we reconstruct wavefields at all image locations $\mathbf{y}_m$ for every receiver location on the acquisition surface $\mathbf{x}_m$, for every experiment, i.e. construct solutions of the wave-equation for every trace on the surface acting as an independent source (number of $\mathbf{x}_m$ receivers solutions to the acoustic wave-equation). This is an unaffordable operation in complex media.

In contrast, imaging functional (3) achieves statistical stability by cross-correlating and averaging wavefields parametrized function of the image location. In this functional, the wavefields subject to cross-correlation are $\overline{U_S(\mathbf{x}_s,\mathbf{y}_m\pm\mathbf{y}_h,\omega_m\pm\omega_h)}\int\limits_{\mathbf{x}_m} d\mathbf{x}_m\, U_R(\mathbf{x}_m,\mathbf{y}_m\pm\mathbf{y}_h,\omega_m\pm\omega_h)$. This

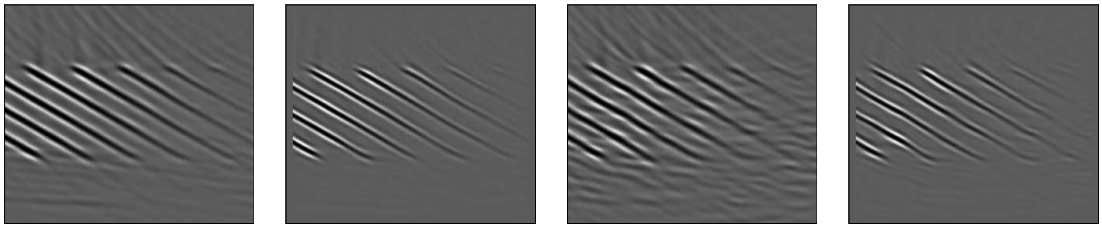

(a) (b) (c) (d)

Figure 5: Zoom-in on the images for example shown in figures 4(a)-4(d): imaging data simulated in background media using CIC (a) and IIC (b). imaging data simulated in random media using CIC (c) and IIC (d).

operation requires that we reconstruct wavefields at all image locations $\mathbf{y}_m$ for all receiver locations on the surface $\mathbf{x}_m$, for every experiment. The cost associated with this operation is comparable with the cost of conventional imaging, i.e. construct solutions of the wave-equation for all trace on the surface acting as simultaneous sources (one solution to the acoustic wave-equation). This is an affordable operation in complex media.

STATISTICAL STABILITY

By statistical instability we mean that images obtained for different realizations of random models with the identical statistics are different. Figures 2(a)-2(c) illustrate data modeled for different realizations of a velocity model. The general kinematics of the data are the same, but subtle differences exist between the various datasets due to the random model variations. Migration using conventional imaging condition leads to the images in figures 2(d)-2(f) which show variations from realization to realization. In contrast, figures 2(g)-2(i) show images obtained by the interferometric imaging condition which are more similar to one-another since many of the artifacts have been attenuated.

In typical seismic imaging problems, we cannot ensure that random velocity fluctuations are small. It is desirable that imaging remains statistically stable even in cases when velocity varies with larger magnitude. We investigate the statistical properties of the imaging functional in equation (3) using numeric experiments similar to the one used earlier. This numeric experiment simulates a situation when the random model fluctuations of comparable scale with the seismic wavelength lead to destruction of the wavefronts, as suggested by the "weak fluctuations" regime and when large magnitude of the random noise leads to diffusion of the wavefronts, as suggested by the "diffusion approximation" regime. This combination of parameters could be regarded as a worst-case-scenario from a theoretical standpoint.

Figures 3(a)-3(c) show data sets modeled with a velocity model with increasingly strong random noise, up to 30% of the background. Migration using conventional imaging condition leads to the images in figures 3(d)-3(f), showing artifacts due to defocusing caused by the unknown random fluctuations in the model. However, migration using the interferometric imaging condition leads to the images in figures 3(g)-3(i) where the artifacts are attenuated.

EXAMPLE

One application of the interferometric imaging condition is imaging in complex media characterized by unknown random variations. Consider the model depicted in figures 4(a)-4(b). The left panels depict the known smooth velocity v_0, and the right panels depict the model with random variations. The imaging target is located around $z = 700$ m. We model data with random velocity and image using the smooth model. Figures 4(a)-4(b) show wavefield snapshots in the two models.

Migration with conventional imaging condition of the data simulated in the smooth model using the smooth velocity produces the images in figure 5(a). The target is well imaged, although the image shows artifacts due to truncation of the data on the acquisition surface. In contrast, migration with the conventional imaging condition of the data simulated in the random model using the smooth velocity produces the images in figure 5(c). The image is distorted by the random variations in the model that are not accounted for in the smooth migration velocity. The target is harder to discern since it overlaps with many truncation and defocusing artifacts caused by the inaccurate migration velocity.

Figure 5(b) shows the image for the same situation as the one depicted in figure 5(a), except that migration uses the interferometric imaging condition (3). In this situation, since we are using the same model for modeling and migration, the interferometric imaging condition is not expected to change the image much. Interestingly, some of the truncation artifacts are attenuated, but otherwise the images are similar and the targets are easy to identify. Similarly, figure 5(d) shows the migrated image for the same situation as the one depicted in figure 5(c), with migration using the interferometric imaging condition (3). Many of the artifacts caused by the inaccurate velocity model are suppressed and the imaging targets are more clearly visible and easier to interpret. Furthermore, the general patterns of amplitude variation along the imaged reflectors are similar between figures 5(b) and 5(d).

CONCLUSIONS

Conventional seismic imaging conditions based on wavefield cross-correlations are extended to achieve statistical stability for models with rapid, small-scale velocity variations. Random velocity variations on a scale comparable with the seismic wavelength are modeled by correlated Gaussian distributions. Statistical stability is achieved by local averaging of cross-correlated wavefields at image locations. The proposed interferometric imaging condition is a natural extension of and reduces to the conventional cross-correlation imaging condition when the averaging window is made infinitely small. The main characteristic of the method is that it operates on extrapolated wavefields at image positions (thus the name *interferometric imaging condition*), in contrast with alternative approaches involving migration of interferograms obtained by local data cross-correlations based on acquisition surface coordinates.

ACKNOWLEDGMENT

Paul Sava acknowledges the support of the sponsors of the Center for Wave Phenomena at Colorado School of Mines.

REFERENCES

Borcea, L., G. Papanicolaou, and C. Tsogka, 2005, Interferometric array imaging in clutter: Inverse Problems, **21**, 1419–1460.

———, 2006a, Adaptive interferometric imaging in clutter and optimal illumination: Inverse Problems, **22**, 1405–1436.

———, 2006b, Coherent interferometric imaging in clutter: Geopysics, **71**, SI165–SI175.

———, 2006c, Coherent interferometry in finely layered random media: SIAM Journal on Multiscale Modeling and Simulation, **5**, 62–83.

Claerbout, J. F., 1985, Imaging the Earth's interior: Blackwell Scientific Publications.

Dussaud, E., 2005, Velocity analysis in the presence of uncertainty: Ph.D. Thesis, Rice University.

Fouque, J., J. Garnier, A. Nachbin, and K. Solna, 2005, Time reversal refocusing for point source in randomly layered media: Wave Motion, **42**, 191–288.

Papanicolaou, G., L. Ryzhik, and K. Solna, 2004, Statistical stability in time reversal: SIAM J. Appl. Math., **64**, 1133–1155.

Pratt, R. G., 1990, Inverse theory applied to multi-source cross-hole tomography. part 2: Elastic wave-equation method: Geophys. Prosp., **38**, 311–312.

Pratt, R. G. and M. H. Worthington, 1990, Inverse theory applied to multi-source cross-hole tomography. part 1: Acoustic wave-equation method: Geophys. Prosp., **38**, 287–310.

Sava, P. and B. Biondi, 2004a, Wave-equation migration velocity analysis - I: Theory: Geophysical Prospecting, **52**, 593–606.

———, 2004b, Wave-equation migration velocity analysis - II: Subsalt imaging examples: Geophysical Prospecting, **52**, 607–623.

Shen, P., W. W. Symes, S. Morton, and H. Calandra, 2005, Differential semblance velocity analysis via shot profile migration: 2249–2253.

Tarantola, A., 1987, Inverse Problem Theory: methods for data fitting and model parameter estimation: Elsevier.

Woodward, M. J., 1992, Wave-equation tomography: Geophysics, **57**, 15–26.